Reconstruction of three-dimensional anisotropic structure from small-angle scattering experiments

Guan-Rong Huang, Yangyang Wang, Bin Wu, Zhe Wang, Changwoo Do, Gregory S. Smith, Wim Bras, Lionel Porcar, Péter Falus, and Wei-Ren Chen

Phys. Rev. E **96**, 022612 — Published 28 August 2017

DOI: 10.1103/PhysRevE.96.022612

On the Reconstruction of Three-Dimensional Anisotropic Structure from Small-Angle Scattering Experiments

Guan-Rong Huang[1,2,3], Yangyang Wang[4],* Bin Wu[3], Zhe Wang[3], Changwoo Do[3], Gregory S. Smith[3], Wim Bras[3], Lionel Porcar[5], Péter Falus[5], and Wei-Ren Chen[2,3†]

[1] *Physics Division, National Center for Theoretical Sciences, Hsinchu 30013, Taiwan, ROC*

[2] *Shull Wollan Center, the University of Tennessee and Oak Ridge National Laboratory, Oak Ridge, TN 37831, USA*

[3] *Biology and Soft Matter Division, Oak Ridge National Laboratory, Oak Ridge, TN 37831, USA*

[4] *Center for Nanophase Materials Sciences, Oak Ridge National Laboratory, Oak Ridge, TN, 37831, USA and*

[5] *Institut Laue-Langevin, B.P. 156, F-38042 Grenoble CEDEX 9, France*

(Dated: August 3, 2017)

When subjected to flow, the structures of many soft matter systems become anisotropic due to the symmetry breaking of the spatial arrangements of constituent particles at the microscopic level. While it has now been a common practice to use various small angle scattering techniques to explore the flow-induced microstructural distortion, how the three-dimensional anisotropic structure can be faithfully reconstructed from the two-dimensional small-angle scattering spectra has not been thoroughly discussed in the literature. In this work, we rigorously address this issue from a mathematical perspective by using real spherical harmonic expansion analysis. We first show that, except for the cases where the mechanical perturbation is sufficiently small, the existing small-angle scattering techniques in general do not provide the complete information of structural distortion. This limitation is caused by the linear dependence of certain spherical harmonic basis vectors on the flow-vorticity and flow-velocity gradient planes in the Couette shear cell. To circumvent the constraint imposed by this geometry, an alternative approach by using a parallel sliding plate shear cell with a central rotary axis along the flow direction is proposed. From the calculation of rotation of reference frame, we demonstrate the feasibility of this experimental implementation for fully resolving three-dimensional anisotropic structure via a case study of sheared polymers.

PACS numbers: 61.05.fg, 83.85.Cg, 83.85.Hf

I. INTRODUCTION

The spatial arrangement of the constituent particles of a soft matter system is driven out of the equilibrium configurations under flow and deformation. There has been much scientific as well as technological interest in understanding how the structural distortion at the particle level is connected to the macroscopic rheological properties [1, 2]. Two-point correlation functions, such as the pair distribution function $g(\boldsymbol{r})$ in real space or the inter-particle structure factor $S(\boldsymbol{Q})$ in reciprocal $\boldsymbol{Q}$ space, are of particular interest for rheology of complex fluids, because these quantities can be probed experimentally. They have been extensively used in the theoretical and computational investigations in the past as a vehicle for exploring the microscopic origin of the viscoelastic behavior in non-equilibrium liquids. Recent studies of experiments and theory, on colloidal dispersions, were also able to investigate the 3D structural deformation, using confocal microscopy experiments, Brownian and molecular dynamic simulations, and the mode-coupling theory [3–7].

In order to quantify the structural distortion under different flow conditions, the anisotropic pair distribution function $g(\boldsymbol{r})$ has been expressed in terms of real spherical harmonics (RSH) in a series of computational studies in the past [1, 8–12]. The coefficients associated with different basis vectors, which are related to a number of flow properties such as shear stress and normal stress difference contributed by the inter-particle interaction, can be straightforwardly computed due to the orthogonality of RSH functions in the three-dimensional (3D) space.

Parallel to these computational studies, there has been a considerable amount of experimental effort, mainly from small-angle scattering (SAS) measurements, to investigate the structural evolution of various soft matter systems under various flow conditions in the non-Newtonian regime [13–20]. Unlike computer simulations, the 3D structural information has to be reconstructed from two-dimensional (2D) spectra in small-angle scattering experiments. In the case of uniaxial stretching, we have recently demonstrated that the reconstruction can be accomplished by SAS measurement on a single plane parallel to the stretching direction, due to the cylindrical symmetry of the deformation [21]. However, the reconstruction problem for the shear geometry has not been completely solved. Because of the low symmetry of shear deformation, it is still unclear whether SAS experiments on the conventional flow-vorticity (xz) and flow-velocity gradient (xy) planes can always provide the full information about micro-structural changes.

In this work, we address the aforementioned challenge from a mathematical perspective. We demonstrate that SAS experiments on the xz and xy planes of a Couette cell in general only yield partial information on the 3D

* wangy@ornl.gov

† chenw@ornl.gov

anisotropic structure. The linear dependence among certain RSH basis vectors on these two planes inherently prohibits the full reconstruction when the structural perturbation is large. To bypass this intrinsic constraint of the Couette geometry, we propose an alternative parallel-plate shear cell with a central rotary axis along the flow direction. We show that additional information among the coefficients of the relevant RSH functions can be obtained by tilting the parallel plates, which makes up the underdetermined linear equations originating from the linear dependence of the basis vectors and thus permits full restoration of the 3D distorted structure.

The paper is organized as follows: In Sec. II, we present a detailed analysis of the anisotropic structure obtained from the scattering measurements with the Couette cell and demonstrate the validity and limitation of this geometry for the structural reconstruction via the RSH analysis. We then proceed to introduce the RSH analysis on the non-equilibrium structure factor obtained from the scattering measurements with parallel plates with a rotary axis and demonstrate its capability of extracting the complete information of structural distortion for sheared polymers in Sec. III. Discussions and conclusions are presented in Sec. IV.

II. REAL SPHERICAL HARMONICS EXPANSION OF STRUCTURE FACTOR

First, let us briefly review some of the basics of the real spherical harmonic expansion technique. To investigate the anisotropic properties, in ref. [11] the structure factor of the sample in a rheo-SAS experiment is expanded as a linear combination of RSH:

$$S(\boldsymbol{Q}) = \sum_{l=0}^{\infty} \sum_{m=-l}^{l} S_l^m(Q) Y_l^m(\theta, \phi), \tag{1}$$

where $S(\boldsymbol{Q})$ is the structure factor of molecules, $\boldsymbol{Q}$ is the momentum transfer between the beam and molecules, l and m are both integers, Q is the magnitude of $\boldsymbol{Q}$, $S_l^m(Q)$ are coefficients as a function of Q, θ is the angle with respect to the z-axis, ϕ is the polar angle with respect to x-axis on the xy-plane, and $Y_l^m(\theta, \phi)$ are RSH defined as

$$Y_l^m(\theta,\phi) = \begin{cases} \sqrt{2} A_l^m P_l^{|m|}(\cos\theta)\sin(|m|\phi) & , m < 0 \\ A_l^m P_l^m(\cos\theta) & , m = 0 \\ \sqrt{2} A_l^m P_l^m(\cos\theta)\cos(m\phi) & , m > 0 \end{cases}, \tag{2}$$

where $A_l^m = \sqrt{(2l+1)(l-|m|)!/(l+|m|)!}$ and P_l^m is the associated Legendre polynomials.

Considering the case of shear flow (Fig. 1), where x, y, and z are the direction of flow velocity, velocity gradient, and vorticity, respectively, the $S(\boldsymbol{Q})$ has the symmetrical conditions: $S(Q,\theta,\phi) = S(Q,\pi-\theta,\phi)$ and $S(Q,\theta,\phi) = S(Q,\theta,\phi+\pi)$. This puts restrictions on the values of l and m: the l and m must both be even, since the P_l^m and trigonometric functions satisfy the identities

$$\begin{aligned} P_l^m[\cos(\pi-\theta)] &= (-1)^{l+m} P_l^m(\cos\theta), \\ \sin[m(\phi+\pi)] &= (-1)^m \sin(m\phi), \\ \cos[m(\phi+\pi)] &= (-1)^m \cos(m\phi). \end{aligned} \tag{3}$$

Therefore, the structure factor is simplified as

$$S(\boldsymbol{Q}) = \sum_{l,m:\text{even}} S_l^m(Q) Y_l^m(\theta,\phi). \tag{4}$$

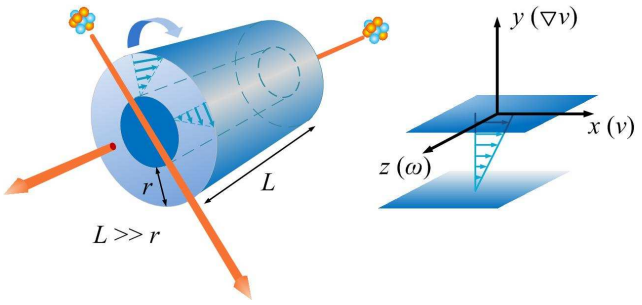

Figure 1. Schematic representation of the Couette cell with the reference frame, where v is velocity, ∇v is velocity gradient, ω is vorticity, and the height L is much larger than the gap r.

In rheo-SAS experiments, one does not have full access to the 3D structure factor, but the cross sections of $S(\boldsymbol{Q})$ on 2D planes. In other words, one now has to deal with 2D basis that are linear dependent on each other. Therefore, the information on different planes is generally needed to determine the spherical harmonic expansion coefficients. To further demonstrate this point, in the following sections we will consider the truncation of real spherical harmonic expansion (RSHE) at $l = 2$ and $l = 4$, respectively. For the sake of simplicity, the following shorthand notations will be used in our discussion:

$$\begin{gathered} S_l^m \equiv S_l^m(Q),\ Y_l^m \equiv Y_l^m(\theta,\phi),\ \xi \equiv \cos\theta, \\ Y_{xy}^{l,m} \equiv Y_l^m(\pi/2,\phi),\ Y_{xz}^{l,m} \equiv Y_l^m(\theta,\phi=0,\pi/2), \\ Y_{yz}^{l,m} \equiv Y_l^m(\theta,\phi=\pi/2,3\pi/2). \end{gathered}$$

Coefficient Extraction for Real Spherical Harmonics Expansion Truncated at $l = 2$

When the degree of microscopic deformation is small, it suffices to truncate the real spherical harmonic expansion at $l = 2$:

$$S(\boldsymbol{Q}) = S_0^0 Y_0^0 + S_2^{-2} Y_2^{-2} + S_2^0 Y_2^0 + S_2^2 Y_2^2. \tag{5}$$

It is easy to see that the structure factor on the xy-plane ($\theta = \pi/2$) is

$$\begin{aligned} S(Q,\theta=\pi/2,\phi) &\equiv S_{xy}(Q,\phi) = \textstyle\sum_{l,m} S_l^m Y_{xy}^{l,m} \\ &= S_0^0 - \tfrac{\sqrt{5}}{2} S_2^0 + \tfrac{\sqrt{15}}{2} S_2^2 \cos(2\phi) + \tfrac{\sqrt{15}}{2} S_2^{-2} \sin(2\phi), \end{aligned} \tag{6}$$

where the four unknown coefficients require four linear independent equations (LIEs) to be solved. These equations can be found by carrying out the weighting integral of $S_{xy}(Q,\phi)$ and $Y_{xy}^{l,m}$ with respect to ϕ

$$S_{xy}^{l,m} \equiv \frac{1}{2\pi}\int_0^{2\pi} S_{xy}(Q,\phi)Y_l^m(\phi)d\phi. \tag{7}$$

As a consequence,

$$\begin{aligned} S_{xy}^{0,0} &= S_0^0 - \tfrac{\sqrt{5}}{2}S_2^0, \\ S_{xy}^{2,2} &= \tfrac{15}{8}S_2^2, \\ S_{xy}^{2,-2} &= \tfrac{15}{8}S_2^{-2}. \end{aligned} \tag{8}$$

Since $Y_{xy}^{0,0}$ and $Y_{xy}^{2,0}$ basis are coupled together on xy-plane, carrying out $S_{xy}^{2,0}$ will yield no more information. To get more information of structure factor, we should seek to the 2D signal on other planes. On the xz-plane, the structure factor truncated at $l=2$ is

$$\begin{aligned} &S(Q,\theta,\phi=0) \equiv S_{xz}(Q,\theta) = \textstyle\sum_{l,m} S_l^m Y_{xz}^{l,m} \\ &= S_0^0 + \tfrac{\sqrt{5}}{2}S_2^0(3\cos^2\theta - 1) + \tfrac{\sqrt{15}}{2}S_2^2\sin^2\theta \end{aligned} \tag{9}$$

Similarly, we have the following weighting integral(s) of $S_{xz}(Q,\theta)$ and $Y_{xz}^{l,m}$ with respect to θ

$$\begin{aligned} S_{xz}^{l,m} &\equiv \tfrac{1}{2}\textstyle\int_0^{\pi} S_{xz}(Q,\theta)Y_{xz}^{l,m}\sin\theta d\theta \\ &= \tfrac{1}{2}\textstyle\int_{-1}^{1} S_{xz}(Q,\xi)Y_{xz}^{l,m}d\xi. \end{aligned} \tag{10}$$

Therefore,

$$S_{xz}^{0,0} = S_0^0 + \sqrt{\tfrac{5}{3}}S_2^2. \tag{11}$$

We emphasize that the left-hand sides of Eqs. (8) and (11) are quantities that could be accessed experimentally. After some straightforward algebraic calculations, we can explicitly express S_l^m in terms of the weighting integrals:

$$\begin{aligned} S_0^0 &= S_{xz}^{0,0} - \tfrac{8}{3\sqrt{15}}S_{xy}^{2,2}, \\ S_2^0 &= \tfrac{2}{\sqrt{5}}S_{xz}^{0,0} - \tfrac{16}{15\sqrt{3}}S_{xy}^{2,2} - \tfrac{2}{\sqrt{5}}S_{xy}^{0,0}, \\ S_2^2 &= \tfrac{8}{15}S_{xy}^{2,2}, \\ S_2^{-2} &= \tfrac{8}{15}S_{xy}^{2,-2}. \end{aligned} \tag{12}$$

Equation (11) is valid for the systems with small structural perturbation. It should be noted that S_2^0 and S_2^{-2} can be measured on xy-plane alone without additional information from the xz-plane. Together, the SAS measurements on the xz- and xy-planes are sufficient for the extraction of all the S_l^m, provided $S(\boldsymbol{Q})$ can be truncated at $l=2$. Experimentally, however, it is generally difficult to measure the structure on the xy-plane, due to technical challenges such as multiple scattering.

Coefficient Extraction for Real Spherical Harmonics Expansion Truncated at $l=4$

As the microscopic deformation becomes larger, the RSHE truncated at $l=2$ can no longer precisely describe the scattering spectrum. For example, the $l=4$ term of cubic symmetry can be significant for soft-sphere systems [11]. In such a case, we should consider the RSHE of $S(\boldsymbol{Q})$ up to $l=4$:

$$\begin{aligned} S(\boldsymbol{Q}) = {} & S_0^0Y_0^0 + S_2^{-2}Y_2^{-2} + S_2^0Y_2^0 + S_2^2Y_2^2 + S_4^{-4}Y_4^{-4} \\ & + S_4^{-2}Y_4^{-2} + S_4^0Y_4^0 + S_4^2Y_4^2 + S_4^4Y_4^4, \end{aligned} \tag{13}$$

with 9 undetermined expansion coefficients. As we shall show below, it is not feasible to extract all S_l^m coefficients on the convectional planes, namely the xy, xz, and yz planes, where only 8 LIEs can be established.

The structure factor on xy-plane is

$$\begin{aligned} S_{xy}(Q,\phi) = {} & S_0^0 - \tfrac{\sqrt{5}}{2}S_2^0 + \tfrac{9}{8}S_4^0 + (\tfrac{\sqrt{15}}{2}S_2^2 - \tfrac{3\sqrt{5}}{4}S_4^2)\cos(2\phi) \\ & + (\tfrac{\sqrt{15}}{2}S_2^{-2} - \tfrac{3\sqrt{5}}{4}S_4^{-2})\sin(2\phi) + \tfrac{3\sqrt{35}}{8}S_4^{-4}\sin(4\phi) \\ & + \tfrac{3\sqrt{35}}{8}S_4^4\cos(4\phi), \end{aligned} \tag{14}$$

which is a Fourier series with the five linear independent basis: $[1,\cos(2\phi),\cos(4\phi),\sin(2\phi),\sin(4\phi)]$. In other words, no matter what weighting function we use, the resulting weighting integrals can yield at most 5 LIEs, due to the coupling of RSH on the xy-plane. Similar to the situation of $l=2$, from the weighting integrals, we have

$$\begin{aligned} S_{xy}^{0,0} &= S_0^0 - \tfrac{\sqrt{5}}{2}S_2^0 + \tfrac{9}{8}S_4^0, \\ S_{xy}^{2,2} &= \tfrac{15}{8}S_2^2 - \tfrac{15\sqrt{3}}{16}S_4^2, \\ S_{xy}^{2,-2} &= \tfrac{15}{8}S_2^{-2} - \tfrac{15\sqrt{3}}{16}S_4^{-2}, \\ S_{xy}^{4,4} &= \tfrac{315}{128}S_4^4, \\ S_{xy}^{4,-4} &= \tfrac{315}{128}S_4^{-4}. \end{aligned} \tag{15}$$

On the other hand, the structure factor on the xz-plane is

$$\begin{aligned} S_{xz}(Q,\theta) = {} & S_0^0 + \sqrt{5}S_2^0P_2^0(\xi) + \sqrt{\tfrac{5}{12}}S_2^2P_2^2(\xi) \\ & + 3S_4^0P_4^0(\xi) + \tfrac{\sqrt{5}}{10}S_4^2P_4^2(\xi) + \tfrac{\sqrt{35}}{280}S_4^4P_4^4(\xi). \end{aligned} \tag{16}$$

On the xz-plane, $[Y_{xz}^{0,0}, Y_{xz}^{2,0}, Y_{xz}^{2,2}, Y_{xz}^{4,0}, Y_{xz}^{4,2}, Y_{xz}^{4,4}]$ form a linear dependent set that can be expressed in terms of three proper basis of them. For example,

$$\begin{aligned} Y_{xz}^{2,2} &= \tfrac{\sqrt{15}}{3}Y_{xz}^{0,0} - \tfrac{1}{\sqrt{3}}Y_{xz}^{2,0}, \\ Y_{xz}^{4,2} &= \tfrac{1}{\sqrt{5}}Y_{xz}^{0,0} + Y_{xz}^{2,0} - \tfrac{2}{\sqrt{5}}Y_{xz}^{4,0}, \\ Y_{xz}^{4,4} &= \tfrac{7}{\sqrt{35}}Y_{xz}^{0,0} - \tfrac{2}{\sqrt{7}}Y_{xz}^{2,0} + \tfrac{1}{\sqrt{35}}Y_{xz}^{4,0}. \end{aligned} \tag{17}$$

Alternatively, this can be verified by computing the rank of the matrix whose elements are the coefficients of ξ power in $Y_{xz}^{l,m}(\xi)$. Since the rank of the matrix rank is 3, we confirm that this set contains three linear independent basis. Therefore, measurements on the xz-plane provide the following three equations from the weighting integrals with respect to ξ

$$\begin{aligned} S_{xz}^{0,0} &= S_0^0 + \sqrt{\tfrac{5}{3}}S_2^2 + \sqrt{\tfrac{1}{5}}S_4^2 + \sqrt{\tfrac{7}{5}}S_4^4, \\ S_{xz}^{2,0} &= S_2^0 - \sqrt{\tfrac{1}{3}}S_2^2 + S_4^2 - \sqrt{\tfrac{4}{7}}S_4^4, \\ S_{xz}^{4,0} &= S_4^0 - \tfrac{2}{\sqrt{5}}S_4^2 + \tfrac{1}{\sqrt{35}}S_4^4. \end{aligned} \tag{18}$$

However, the equation of $S_{xz}^{4,0}$ is linear dependent to the other seven LIEs and should be removed. To get a complete set of nine LIEs, one might want to examine the structure factor on the yz-plane to gain the remaining two. In particular, an additional equation is needed to decouple S_2^{-2} and S_4^{-2}. However, this turns out to be impossible because the structure factor on yz-plane ($\phi = \pi/2, 3\pi/2$) is

$$S_{yz}(Q,\theta) = S_0^0 + \sqrt{5}S_2^0 P_2^0(\xi) - \sqrt{\tfrac{5}{12}}S_2^2 P_2^2(\xi) + 3S_4^0 P_4^0(\xi) - \tfrac{\sqrt{5}}{10}S_4^2 P_4^2(\xi) + \tfrac{\sqrt{35}}{280}S_4^4 P_4^4(\xi), \quad (19)$$

which will produce the LIEs, from the weighting integrals, with the same S_l^m terms as those of $S_{xz}^{l,m}$. Since neither Eq. (16) nor Eq. (19) contains S_2^{-2} and S_4^{-2}, these coefficients cannot be determined. In other words, S_2^{-2} and S_4^{-4} are coupled together on the xy-plane and disappear on the xz- and yz- planes. From the yz-plane, we obtain an additional LIE for the other coefficients:

$$S_{yz}^{4,0} = \frac{1}{2}\int_{-1}^{1} S_{yz}(Q,\xi)Y_{yz}^{4,0}d\xi = S_4^0 + \frac{2}{\sqrt{5}}S_4^2 + \frac{1}{\sqrt{35}}S_4^4. \quad (20)$$

Combining Eqs. (15), (18), and (20), we arrive at the following solutions for S_l^m:

$$\begin{aligned}
S_0^0 &= \tfrac{7}{9}S_{xy}^{0,0} + \tfrac{4\sqrt{15}}{135}S_{xy}^{2,2} + \tfrac{2}{9}A_1 + \tfrac{7\sqrt{5}}{18}A_2 - \tfrac{7}{8}A_3,\\
S_2^0 &= \tfrac{\sqrt{5}}{9}S_{xy}^{0,0} + \tfrac{44\sqrt{3}}{135}S_{xy}^{2,2} - \tfrac{\sqrt{5}}{9}A_1 + \tfrac{23}{18}A_2 - \tfrac{\sqrt{5}}{8}A_3,\\
S_2^2 &= -\tfrac{\sqrt{15}}{9}S_{xy}^{0,0} + \tfrac{4}{45}S_{xy}^{2,2} + \tfrac{\sqrt{15}}{9}A_1 - \tfrac{5\sqrt{3}}{18}A_2 + \tfrac{\sqrt{15}}{8}A_3,\\
S_4^{-4} &= \tfrac{128}{315}S_{xy}^{4,-4}\\
S_4^0 &= \tfrac{4}{9}S_{xy}^{0,0} + \tfrac{16\sqrt{15}}{135}S_{xy}^{2,2} - \tfrac{4}{9}A_1 + \tfrac{2\sqrt{5}}{9}A_2 + \tfrac{1}{2}A_3,\\
S_4^2 &= -\sqrt{5}(\tfrac{2}{9}S_{xy}^{0,0} + \tfrac{8\sqrt{15}}{135}S_{xy}^{2,2} - \tfrac{2}{9}A_1 + \tfrac{\sqrt{5}}{9}A_2 - \tfrac{1}{4}A_3),\\
S_4^4 &= \tfrac{128}{315}S_{xy}^{4,4},\\
2S_2^{-2} - \sqrt{3}S_4^{-2} &= \tfrac{16}{15}S_{xy}^{2,-2}, \quad (21)
\end{aligned}$$

where $A_1 = S_{xz}^{0,0} - \frac{128\sqrt{35}}{1575}S_{xy}^{4,4}$, $A_2 = S_{xz}^{2,0} + \frac{256\sqrt{7}}{2205}S_{xy}^{4,4}$, and $A_3 = S_{yz}^{4,0} - \frac{128\sqrt{35}}{11025}S_{xy}^{4,4}$. For the experimental measurements on these three planes, the explicit formula of Eq. (21) can act as a convenient tool for experimetalists to extract the available information. We see that for RSHE truncated at $l = 4$, S_4^{-4} and S_4^4 can be determined by SAS measurement on the xy-plane alone. All the three planes, xy, xz, and yz are needed for S_0^0, S_2^0, S_2^2, S_4^0, and S_4^2, while S_2^{-2} and S_4^{-2} clearly cannot be separated.

We note that in Ref. [19], 12 linear equations are implicitly used to numerically extract all the 9 coefficients S_l^m of RSHE truncated at $l = 4$. However, as we have demonstrated mathematically, this cannot possibly be done without invoking additional assumptions. Eq. (21) tells us that S_2^{-2} can be drawn out of the xy-plane only when S_4^{-2} is much smaller than S_2^{-2}, which is actually valid for the system with small perturbation. However, once higher order terms are needed for a full description of the structural changes, e.g. for high shear rates and shear strains, measurements on the conventional planes become inadequate. Moreover, the long path length (> 5 mm) for the xy-plane measurement often leads to multiple scattering, and the cross section of S_l^m with $m < 0$ on yz-plane is nearly zero, making it difficult to carry out experiments on these two planes. To overcome these difficulties, we propose to use the parallel-plate sliding cell tilted at different angles to obtain information on unconventional planes as shown in Fig. 2. Consequently, a new data analysis method for this cell geometry need to developed. In the next section, the rotation of reference frame is introduced to resolve all the S_l^m coefficients up to $l = 4$, providing a useful tool for investigating the microscopic mechanism of soft matter systems under flow and deformation.

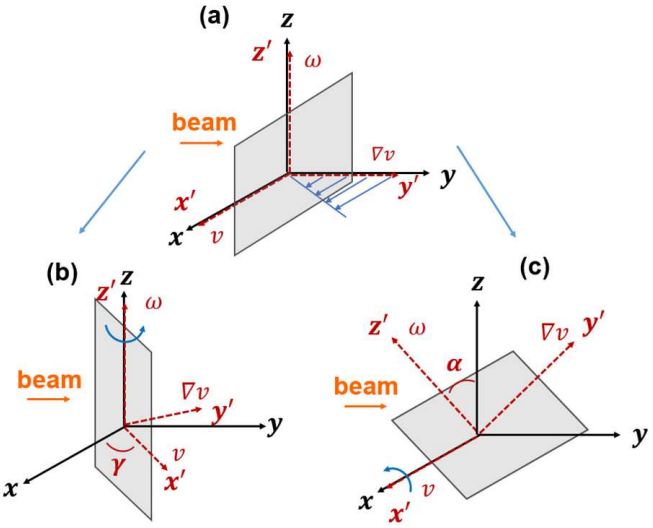

Figure 2. Schematic representation of the coordinate system set-up. (a) Reference frames for plate cell $[x', y', z']$ and sample $[x, y, z]$. (b) The rotation of plate cell about x-axis at an angle α. (c) The rotation of plate about z-axis at an angle α.

III. ROTATION TRANSFORMATION OF REAL SPHERICAL HARMONICS

Considering the case, the incident beam is along the y-axis, and the parallel-plate cell lies on the xz-plane as shown in Fig. 2(a). The direction of flow velocity, velocity gradient, and vorticity are x, y, and z, respectively. Due to the constraint of the cell and data analysis in rheo-SAS experiments, measurements on the xy-plane and yz-plane are intrinsically complicated due to problems such as multiple scattering arising from the long path length. Therefore, it is highly desired to extract structural information from other unconventional planes, by rotating xz-plane about x-axis or z-axis by an angle α or γ (Fig. 2(b) and (c)). In experiments, this oper-

ation corresponds to the rotation of the shear cell. As we shall see below, this cell rotation approach is not only feasible but also beneficial for rheo-SAS experiments and subsequent data analysis. For the sake of simplicity, we introduce the following vector notations for S_l^m and Y_l^m:

$$\begin{aligned}\vec{S}_{l=2} &= [S_2^{-2}, S_2^0, S_2^2],\\ \vec{Y}_{l=2} &= [Y_2^{-2}, Y_2^0, Y_2^2],\\ \vec{S}_{l=4} &= [S_4^{-4}, S_4^{-2}, S_4^0, S_4^2, S_4^4],\\ \vec{Y}_{l=4} &= [Y_4^{-4}, Y_4^{-2}, Y_4^0, Y_4^2, Y_4^4].\end{aligned} \tag{22}$$

Hence, the structure factor truncated at $l = 4$ can be re-written as

$$S(\boldsymbol{Q}) = S_0^0 Y_0^0 + \vec{S}_{l=2}\vec{Y}_{l=2}^t + \vec{S}_{l=4}\vec{Y}_{l=4}^t, \tag{23}$$

where t is the symbol of matrix transpose. We note that in this expression the $l \geq 2$ coefficients are the anisotropic terms whereas the isotropic S_0^0 is invariant under rotation transformation.

Rotation of Reference Frame

First, let us consider the passive rotation in Fig. 2(b), about z-axis by an angle γ, which transforms original coordinates $[x, y, z]$ into new coordinates $[x', y', z']$. The transformation, which does not alter the molecular symmetry of soft matter systems under steady shear flow, can be expressed by matrix multiplication

$$\begin{bmatrix} x' \\ y' \\ z' \end{bmatrix} = \begin{bmatrix} \cos\gamma & \sin\gamma & 0 \\ -\sin\gamma & \cos\gamma & 0 \\ 0 & 0 & 1 \end{bmatrix} \begin{bmatrix} x \\ y \\ z \end{bmatrix} \tag{24}$$

Correspondingly, the original Y_l^m in $[x, y, z]$ frame are transformed into a new set of RSH, $\hat{Y}_l^m$, in $[x', y', z']$ frame. For a given l, $\hat{Y}_l^{m'}$ and Y_l^m are related through the following matrix multiplication [22, 23]:

$$\vec{\hat{Y}}_l^t = \vec{R}_z^l(\gamma)\vec{Y}_l^t = \vec{C}^l \vec{D}_l^t(0, 0, \gamma)(\vec{C}^l)^\dagger \vec{Y}_l^t, \tag{25}$$

where $\vec{D}_l^t(0, 0, \gamma)$ is the Wigner D function in the zyz convection of Euler angles [24], † is the symbol of conjugate transpose, and

$$\vec{C}^l = \frac{1}{\sqrt{2}} \begin{bmatrix} i & 0 & \cdots & 0 & \cdots & 0 & (-i)^{2l+1} \\ 0 & i & \cdots & 0 & \cdots & (-i)^{2l-1} & 0 \\ \vdots & \vdots & \ddots & \vdots & \iddots & \vdots & \vdots \\ 0 & 0 & \cdots & \sqrt{2} & \cdots & 0 & 0 \\ \vdots & \vdots & \iddots & \vdots & \ddots & \vdots & \vdots \\ 0 & 1 & \cdots & 0 & \cdots & (-1)^{l-1} & 0 \\ 1 & 0 & \cdots & 0 & \cdots & 0 & (-1)^l \end{bmatrix}. \tag{26}$$

Since the z-rotation preserves the molecular symmetries, i.e., $S(Q, \theta, \phi) = S(Q, \pi - \theta, \phi)$ and $S(Q, \theta, \phi) = S(Q, \theta, \phi + \pi)$, in the $[x', y', z']$ coordinates the $[l, m]$ must still be positive even or zero. The dimensions of $\vec{R}_z^l(\gamma)$ can be narrowed down from $(2l + 1) \times (2l + 1)$ to $(l + 1) \times (l + 1)$ in our calculation. Therefore, the transformation can be written as

$$\begin{aligned}\hat{Y}_0^0 &= Y_0^0,\\ \vec{\hat{Y}}_{l=2} &= \vec{R}_z^{l=2}(\gamma)\vec{Y}_{l=2},\\ \vec{\hat{Y}}_{l=4} &= \vec{R}_z^{l=4}(\gamma)\vec{Y}_{l=4},\end{aligned} \tag{27}$$

where $\vec{R}_z^{l=2}(\gamma)$ and $\vec{R}_z^{l=4}(\gamma)$ are 3×3 and 5×5 matrices, respectively:

$$\vec{R}_z^{l=2}(\gamma) = \begin{bmatrix} \cos 2\gamma & 0 & -\sin 2\gamma \\ 0 & 1 & 0 \\ \sin 2\gamma & 0 & \cos 2\gamma \end{bmatrix},$$

$$\vec{R}_z^{l=4}(\gamma) = \begin{bmatrix} \cos 4\gamma & 0 & 0 & 0 & -\sin 4\gamma \\ 0 & \cos 2\gamma & 0 & -\sin 2\gamma & 0 \\ 0 & 0 & 1 & 0 & 0 \\ 0 & \sin 2\gamma & 0 & \cos 2\gamma & 0 \\ \sin 4\gamma & 0 & 0 & 0 & \cos 4\gamma \end{bmatrix}. \tag{28}$$

Next, we consider the rotation in Fig. 2(c), about x-axis by an angle α, which is much more complicated than the z-rotation since the molecular symmetries are broken under x-rotation. The passive transformation between $[x', y', z']$ and $[x, y, z]$ is

$$\begin{bmatrix} x' \\ y' \\ z' \end{bmatrix} = \begin{bmatrix} 1 & 0 & 0 \\ 0 & \cos\alpha & \sin\alpha \\ 0 & -\sin\alpha & \cos\alpha \end{bmatrix} \begin{bmatrix} x \\ y \\ z \end{bmatrix}. \tag{29}$$

The corresponding x-rotation transformation of RSH is

$$\vec{R}_x^l(\alpha) = \vec{C}^l \vec{D}_l^t(-\pi/2, \alpha, \pi/2)(\vec{C}^l)^\dagger, \tag{30}$$

since a series of zyz rotation, at the angles: $\pi/2$, α, and $-\pi/2$, respectively, yields the rotation about x-axis at an angle α. For the sake of simplicity, $\cos(n\alpha)$ and $\sin(n\alpha)$ are denoted as c_n and s_n, respectively, where $n = 1, 2, 3, 4$. The corresponding x-rotation matrices for $l = 2$ and $l = 4$ are

$$\vec{R}_x^{l=2}(\alpha) = \begin{bmatrix} c_1 & 0 & 0 & s_1 & 0 \\ 0 & c_2 & \frac{\sqrt{3}}{2}s_2 & 0 & \frac{s_2}{2} \\ 0 & -\frac{\sqrt{3}}{2}s_2 & \frac{3c_1^2-1}{2} & 0 & -\frac{\sqrt{3}}{2}s_1^2 \\ -s_1 & 0 & 0 & c_1 & 0 \\ 0 & -\frac{s_2}{2} & -\frac{\sqrt{3}}{2}s_1^2 & 0 & \frac{c_1^2+1}{2} \end{bmatrix},$$

$$\vec{R}_x^{l=4}(\alpha) = \begin{bmatrix} \vec{R}_{x1}^{l=4} & \vec{R}_{x2}^{l=4} & \vec{R}_{x3}^{l=4} \end{bmatrix},$$

$$\vec{R}_{x1}^{l=4} = \begin{bmatrix} \frac{c_1(c_1^2+1)}{2} & 0 & \frac{\sqrt{7}c_1(c_1^2-1)}{2} \\ 0 & \frac{3c_1^2+4c_1^4-3}{4} & 0 \\ -\frac{\sqrt{7}}{2}c_1 s_1^2 & 0 & \frac{c_1(7c_1^2-5)}{2} \\ 0 & \frac{\sqrt{7}(2c_2^2-c_2-1)}{8} & 0 \\ 0 & \frac{\sqrt{70}s_1^3 c_1}{4} & 0 \\ \frac{\sqrt{14}}{4}s_1^3 & 0 & \frac{\sqrt{2}s_1(7s_1^2-6)}{4} \\ 0 & \frac{-\sqrt{14}}{2}s_1 c_1^3 & 0 \\ \frac{\sqrt{2}}{4}s_3 & 0 & \frac{\sqrt{14}(s_3-2s_1)}{4} \\ 0 & \frac{-\sqrt{2}(14s_2+s_4)}{32} & 0 \end{bmatrix},$$

$$\vec{R}^{l=4}_{x2}=\begin{bmatrix} 0 & 0 & \frac{-\sqrt{14}s_1^3}{4} \\ \frac{\sqrt{7}(2c_2^2-c_2-1)}{8} & \frac{-\sqrt{70}s_1^3c_1}{4} & 0 \\ 0 & 0 & \frac{\sqrt{2}s_1(6-7s_1^2)}{4} \\ \frac{28c_1^4-27c_1^2+3}{4} & \frac{\sqrt{10}s_2(7c_1^2-3)}{8} & 0 \\ \frac{\sqrt{10}s_2(3-7c_1^2)}{8} & \frac{35c_1^4-30c_1^2+3}{8} & 0 \\ 0 & 0 & \frac{c_1(7c_1^2-3)}{4} \\ \frac{\sqrt{2}(2s_2-7s_4)}{16} & \frac{\sqrt{5}s_1^2(7s_1^2-6)}{4} & 0 \\ 0 & 0 & \frac{3\sqrt{7}c_1(c_1^2-1)}{4} \\ \frac{\sqrt{14}(2s_2-s_4)}{32} & \frac{\sqrt{35}s_1^4}{8} & 0 \end{bmatrix},$$

$$\vec{R}^{l=4}_{x3}=\begin{bmatrix} 0 & \frac{-\sqrt{2}s_3}{4} & 0 \\ \frac{\sqrt{14}s_1c_1^3}{2} & 0 & \frac{14s_2+s_4}{16\sqrt{2}} \\ 0 & \frac{\sqrt{14}s_1(2-3s_1^2)}{4} & 0 \\ \frac{\sqrt{2}(7s_4-2s_2)}{16} & 0 & \frac{7(s_4-2s_2)}{16\sqrt{14}} \\ \frac{\sqrt{5}s_1^2(7s_1^2-6)}{4} & 0 & \frac{\sqrt{35}s_1^4}{8} \\ 0 & \frac{3\sqrt{7}c_1(c_1^2-1)}{4} & 0 \\ \frac{7c_1^4-6c_1^2+1}{2} & 0 & \frac{\sqrt{7}(c_1^4-1)}{4} \\ 0 & \frac{c_1(9c_1^2-5)}{4} & 0 \\ \frac{\sqrt{7}(c_1^4-1)}{4} & 0 & \frac{c_1^4+6c_1^2+1}{8} \end{bmatrix}. \quad (31)$$

Coefficient Extraction by Rotation Transformation

Having established the basic language for describing the rotation of the reference frame, let us now turn our attention to the determination of expansion coefficients. In the lab frame of Fig. 2, the beam direction is along the y-direction, collecting the structural information of the sample on the xz-plane. Considering a parallel sliding plate cell tilted at an angle with respect to z-axis or x-axis, one can rotate $[x, y, z]$ coordinates about z-axis or x-axis into $[x', y', z']$ coordinates to place the shear cell right on the $x'z'$-plane. In the $[x', y', z']$ frame, the structure factor is

$$\begin{aligned} S(\boldsymbol{Q}) &= S_0^0\hat{Y}_0^0 + \vec{S}_{l=2}\vec{\hat{Y}}^t_{l=2} + \vec{S}_{l=4}\vec{\hat{Y}}^t_{l=4} \\ &= S_0^0Y_0^0 + \vec{S}_{l=2}\vec{R}^{l=2}\vec{Y}^t_{l=2} + \vec{S}_{l=4}\vec{R}^{l=4}\vec{Y}^t_{l=4}. \end{aligned} \quad (32)$$

For $\alpha = 0$ or $\gamma = 0$, $\vec{\hat{Y}}_{l=2} = \vec{Y}_{l=2}$ and $\vec{\hat{Y}}_{l=4} = \vec{Y}_{l=4}$. The structure factor is invariant under rotation transformation, which involves the transformation between basis in different coordinates. For convenience, we can introduce the following notations, $\vec{S} = [S_0^0, \vec{S}_{l=2}, \vec{S}_{l=4}]$, $\vec{R} = [1, \vec{R}^{l=2}, \vec{R}^{l=4}]$, and $\vec{Y} = [Y_0^0, \vec{Y}_{l=2}, \vec{Y}_{l=4}]$. The $S(\boldsymbol{Q})$ can thus be written as $S(\boldsymbol{Q}) = \vec{S}\vec{R}\vec{Y}^t$. LIEs on the xz-plane can be established by taking weighting integral of $S(\boldsymbol{Q})$ and $Y^{l,m}_{xz}(\xi)$ with respect to ξ

$$S^{l,m}_{xz} = \tfrac{1}{2}\int_{-1}^{1} S_{xz}(Q,\xi)Y^{l,m}_{xz}(\xi)d\xi. \quad (33)$$

Rotation method for l=2

For RSHE up to $l = 2$, we have the following LIEs on the xz-plane

$$\begin{aligned} S^{0,0}_{xz} &= S_0^0 + \sqrt{\tfrac{5}{3}}S_2^2, \\ S^{2,0}_{xz} &= S_2^0. \end{aligned} \quad (34)$$

There are different ways to rotate the shear cell in order to obtain the remaining LIEs for solving all the expansion coefficients.

Rotating the parallel sliding plate cell about x-axis by $\pi/4$ leads to the following structure factor

$$\begin{aligned} S(\boldsymbol{Q}) &= S_0^0\hat{Y}_0^0 + \vec{S}_{l=2}\vec{\hat{Y}}^t_{l=2} \\ &= S_0^0Y_0^0 + \vec{S}_{l=2}\vec{R}^{l=2}_x(\alpha=\tfrac{\pi}{4})\vec{Y}^t_{l=2} \\ &= S_0^0Y^{0,0}_{xz} + \tfrac{(S_2^0-\sqrt{3}S_2^2)}{4}Y^{2,0}_{xz} \\ &+ \tfrac{\sqrt{2}}{2}S_2^{-2}Y^{2,1}_{xz} + \tfrac{(3S_2^2-\sqrt{3}S_2^0)}{4}Y^{2,2}_{xz}, \end{aligned} \quad (35)$$

and hence the corresponding LIEs

$$\begin{aligned} \hat{S}^{2,0}_{xz}(\tfrac{\pi}{4}) &= \tfrac{1}{2}(S_2^0 - \sqrt{3}S_2^2), \\ \hat{S}^{2,1}_{xz}(\tfrac{\pi}{4}) &= \sqrt{2}S_2^{-2}, \end{aligned} \quad (36)$$

where $\hat{S}^{l,m}_{xz}(\alpha)$ is the weighting integral of $S(\boldsymbol{Q})$ and $Y^{l,m}_{xz}$ with respect to ξ on xz-plane for rotating the shear cell about x-axis by an angle α. Therefore, the coefficients of RSHE can be extracted as

$$\begin{aligned} S_0^0 &= S^{0,0}_{xz} + \tfrac{\sqrt{15}}{9}[2\hat{S}^{2,0}_{xz}(\tfrac{\pi}{4}) - S^{2,0}_{xz}], \\ S_2^{-2} &= \tfrac{\sqrt{2}}{2}\hat{S}^{2,1}_{xz}(\tfrac{\pi}{4}), \\ S_2^0 &= S^{2,0}_{xz}, \\ S_2^2 &= \tfrac{1}{3}[S^{2,0}_{xz} - 2\hat{S}^{20}_{xz}(\tfrac{\pi}{4})]. \end{aligned} \quad (37)$$

Rotating the sliding plate cell about the z-axis by $\pi/4$ leads to the following structure factor

$$\begin{aligned} S(\boldsymbol{Q}) &= S_0^0\hat{Y}_0^0 + \vec{S}_{l=2}\vec{\hat{Y}}^t_{l=2} \\ &= S_0^0Y_0^0 + \vec{S}_{l=2}\vec{R}^{l=2}_z(\gamma=\tfrac{\pi}{4})\vec{Y}^t_{l=2} \\ &= S_0^0Y_0^0 + S_2^0Y^{2,0}_{xz} - S_2^{-2}Y^{2,2}_{xz}, \end{aligned} \quad (38)$$

and hence the corresponding LIE

$$\tilde{S}^{0,0}_{xz}(\frac{\pi}{4}) = S_0^0 - \sqrt{\frac{5}{3}}S_2^{-2}, \quad (39)$$

where $\tilde{S}^{l,m}_{xz}(\gamma)$ is the weighting integral of $S(\boldsymbol{Q})$ and $Y^{l,m}_{xz}$ with respect to ξ on the xz-plane for rotating the cell about z-axis by an angle γ.

Rotation method for l=4

For the sake of simplicity, $\vec{R}_z(\gamma)$ and $\vec{R}_x(\alpha)$ are denoted as the z-rotation at an angle γ and the x-rotation at an

angle α, respectively. Similarly, take the integrals with respect to ξ

$$\tilde{S}^{l,m}_{xz}(\gamma) = \tfrac{1}{2}\vec{S}\vec{R}_z(\gamma)\int_{-1}^{1}\vec{Y}^t Y^{l,m}_{xz}d\xi,$$
$$\hat{S}^{l,m}_{xz}(\alpha) = \tfrac{1}{2}\vec{S}\vec{R}_x(\alpha)\int_{-1}^{1}\vec{Y}^t Y^{l,m}_{xz}d\xi. \quad (40)$$

Here we only consider the rotation method about the x-axis. An alternative approach involving rotations about both the x-axis and z-axis will be given in the appendix.

By measuring the SAS spectrum on the xz-plane and subsequently rotating the cell about the x-axis by $\pi/6$ and $\pi/4$, we find the following nine LIEs through the weighting integrals, after removing the linear dependent ones:

$$\begin{aligned}
S^{0,0}_{xz} &= [1,0,0,\sqrt{\frac{5}{3}},0,0,0,\sqrt{\frac{1}{5}},\sqrt{\frac{7}{5}}]\vec{S}^t,\\
S^{2,0}_{xz} &= [0,0,1,-\sqrt{\frac{1}{3}},0,0,0,1,\frac{-2}{\sqrt{7}}]\vec{S}^t,\\
S^{4,0}_{xz} &= [0,0,0,0,0,0,0,1,\frac{-2}{\sqrt{5}},\frac{1}{\sqrt{35}}]\vec{S}^t,\\
\hat{S}^{2,0}_{xz}(\tfrac{\pi}{4}) &= [0,0,\frac{1}{2},\frac{-\sqrt{3}}{2},0,0,\frac{-3\sqrt{5}}{8},\frac{1}{4},\frac{-19\sqrt{7}}{56}]\vec{S}^t,\\
\hat{S}^{2,1}_{xz}(\tfrac{\pi}{4}) &= [0,\sqrt{2},0,0,\frac{5}{2}\sqrt{\frac{3}{14}},\frac{\sqrt{6}}{4},0,0,0]\vec{S}^t,\\
\hat{S}^{4,0}_{xz}(\tfrac{\pi}{4}) &= [0,0,0,0,0,0,0,\frac{1}{4},\frac{-3\sqrt{5}}{10},\frac{17\sqrt{35}}{140}]\vec{S}^t,\\
\hat{S}^{4,1}_{xz}(\tfrac{\pi}{4}) &= [0,0,0,0,\frac{-3}{\sqrt{7}},1,0,0,0]\vec{S}^t,\\
\hat{S}^{2,1}_{xz}(\tfrac{\pi}{6}) &= [0,1,0,0,\frac{13\sqrt{21}}{56},\frac{5\sqrt{3}}{8},0,0,0]\vec{S}^t,\\
\hat{S}^{4,0}_{xz}(\tfrac{\pi}{6}) &= [0,0,0,0,0,0,0,\frac{9}{16},\frac{-3\sqrt{5}}{8},\frac{41\sqrt{35}}{560}]\vec{S}^t. \quad (41)
\end{aligned}$$

Solving this set of LIEs yields the final solutions to $\vec{S}$

$$\begin{aligned}
S^0_0 &= S^{0,0}_{xz} - \frac{\sqrt{5}}{2}S^{2,0}_{xz} + \frac{65}{8}S^{4,0}_{xz}\\
&\quad + \sqrt{5}\hat{S}^{2,0}_{xz}(\tfrac{\pi}{4}) + \frac{13}{2}\hat{S}^{4,0}_{xz}(\tfrac{\pi}{4}) + 14\hat{S}^{4,0}_{xz}(\tfrac{\pi}{6}),\\
S^{-2}_2 &= \frac{7\sqrt{2}}{6}\hat{S}^{2,1}_{xz}(\tfrac{\pi}{4}) + \frac{\sqrt{3}}{4}\hat{S}^{4,1}_{xz}(\tfrac{\pi}{4}) - \frac{4}{3}\hat{S}^{2,1}_{xz}(\tfrac{\pi}{6}),\\
S^0_2 &= \frac{3}{2}S^{2,0}_{xz} - \frac{7\sqrt{5}}{2}S^{4,0}_{xz} - \hat{S}^{2,0}_{xz}(\tfrac{\pi}{4})\\
&\quad - \frac{13\sqrt{5}}{4}\hat{S}^{4,0}_{xz}(\tfrac{\pi}{4}) + 7\sqrt{5}\hat{S}^{4,0}_{xz}(\tfrac{\pi}{6}),\\
S^2_2 &= \frac{\sqrt{3}}{2}S^{2,0}_{xz} - \frac{5\sqrt{15}}{2}S^{4,0}_{xz} - \sqrt{3}\hat{S}^{2,0}_{xz}(\tfrac{\pi}{4})\\
&\quad - \frac{11\sqrt{15}}{4}\hat{S}^{4,0}_{xz}(\tfrac{\pi}{4}) + 5\sqrt{15}\hat{S}^{4,0}_{xz}(\tfrac{\pi}{6}),\\
S^{-4}_4 &= -\frac{\sqrt{42}}{9}\hat{S}^{2,1}_{xz}(\tfrac{\pi}{4}) - \frac{\sqrt{7}}{4}\hat{S}^{4,1}_{xz}(\tfrac{\pi}{4}) + \frac{2\sqrt{21}}{9}\hat{S}^{2,1}_{xz}(\tfrac{\pi}{6}),\\
S^{-2}_4 &= -\frac{\sqrt{6}}{3}\hat{S}^{2,1}_{xz}(\tfrac{\pi}{4}) + \frac{1}{4}\hat{S}^{4,1}_{xz}(\tfrac{\pi}{4}) + \frac{2}{\sqrt{3}}\hat{S}^{2,1}_{xz}(\tfrac{\pi}{6}),\\
S^0_4 &= \frac{33}{8}S^{4,0}_{xz} + \frac{13}{4}\hat{S}^{4,0}_{xz}(\tfrac{\pi}{4}) - 7\hat{S}^{4,0}_{xz}(\tfrac{\pi}{6}),\\
S^2_4 &= \frac{7\sqrt{5}}{4}S^{4,0}_{xz} + 2\sqrt{5}\hat{S}^{4,0}_{xz}(\tfrac{\pi}{4}) - 4\sqrt{5}\hat{S}^{4,0}_{xz}(\tfrac{\pi}{6}),\\
S^4_4 &= \frac{3\sqrt{35}}{8}S^{4,0}_{xz} + \frac{3\sqrt{35}}{4}\hat{S}^{4,0}_{xz}(\tfrac{\pi}{4}) - \sqrt{35}\hat{S}^{4,0}_{xz}(\tfrac{\pi}{6}).
\end{aligned} \quad (42)$$

To summarize, when the real spherical harmonic expansion is truncated at $l = 2$, we can measure the SAS spectrum from the xz plane, rotate the shear cell about the x-axis by $\pi/4$, and carry out additional SAS measurements on the tilted sample. Eq. (37) is the working equation for extracting all the four expansion coefficients from these two planes. In the case of truncation at $l = 4$, our new method is to perform SAS measurement on the xz-plane and subsequently rotate the cell about the x-axis by $\pi/6$ and $\pi/4$, respectively. Eq. (42) can be used to fully resolve the nine coefficients.

Tests with Affine Deformation Model of Polymer

The affine deformation model of polymer can serve as an ideal tool for testing the validity of our cell rotation approach. When the segments of a Gaussian chain deforms affinely on all length scales, the single-chain structure factor (form factor) $S(\boldsymbol{Q})$ under shear deformation is:

$$S(\boldsymbol{Q}) = \tfrac{2}{\eta^2}[\exp(-\eta) + \eta - 1],$$
$$\eta = R^2_{g,0}[(1+g^2)Q^2_x + Q^2_y + Q^2_z + 2gQ_xQ_y], \quad (43)$$

where $R_{g,0}$ is the radius of gyration in equilibrium, g is the strain since γ has denoted as the rotation angle about z-axis, and $[Q_x, Q_y, Q_z] = Q[\sin\theta\cos\phi, \sin\theta\sin\phi, \cos\theta]$. Since we are dealing with an analytical model, each $S^m_l(Q)$ term can be directly computed by the integral

$$S^m_l = \frac{1}{4\pi}\int_0^{2\pi}\int_0^{\pi} S(\boldsymbol{Q})Y^m_l \sin\theta d\theta d\phi. \quad (44)$$

The RSHE spectrum of the affine deformation model predicted by Eq. (44), with $g = 0.3$ and up to $l = 4$ order, is plotted in Fig. 3, where the contribution of each S^m_l term can be evaluated. Under this condition, the ratio of S^m_{l+2} to S^m_l is on the order of 0.1, supporting the truncation at $l = 4$. Next we examine the 2D SAS spectra (Fig. 4) after rotating the sample cell about the x-axis by $\pi/4$ and $\pi/6$, respectively. From the 2D spectra, we can apply Eq. (42) to determine the expansion coefficients

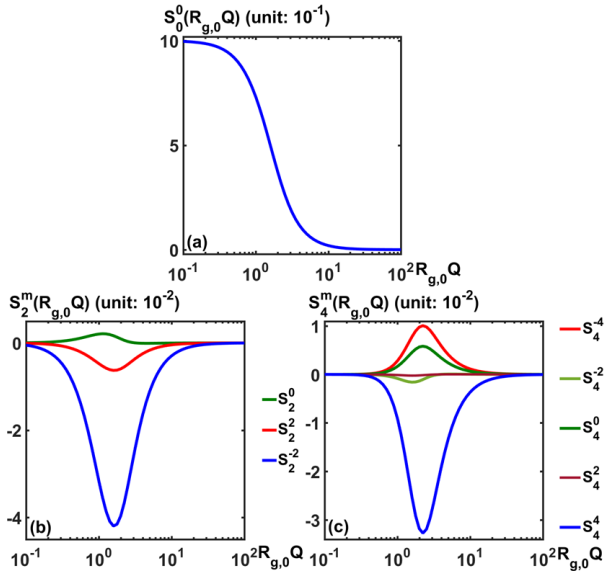

Figure 3. The profile of S_l^m versus $R_{g,0}Q$ in the affine deformation model of polymer. (a) S_0^0 and (b) S_l^m with $l \neq 0$.

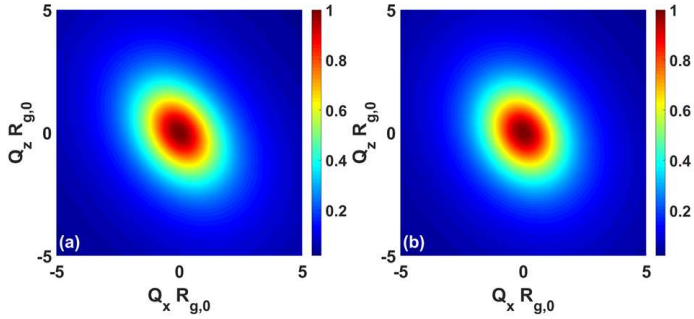

Figure 4. The 2D SAS spectra of rotating sample with $g = 0.5$ on the xz-plane of lab frame: (a) $\hat{S}_{xz}(\frac{\pi}{4})$ and (b) $\hat{S}_{xz}(\frac{\pi}{6})$. Here, the spectra are computed using Eq. (43) with $Q_y = 0$.

S_l^m. Fig. 5 compares these extracted coefficients from $l = 4$ and $l = 2$ RSHE, with those obtained directly from the 3D integral (Eq. (44)). It can be seen that the $l \geq 4$ terms come to play in RSHE spectrum at high strains, and RSHE truncated at $l = 4$ is sufficient to reconstruct the spectrum of S_2^{-2}.

IV. CONCLUDING REMARKS AND SUMMARY

In this work, we have restricted our discussions to the shear geometry. For uniaxial extension, we have previously shown that the spherical harmonic expansion of the single-chain structure factor of a polymer chain has a much simpler form [21]:

$$S(\boldsymbol{Q}) = \sum_{l:\text{even}} S_l^0(Q) Y_l^0(\theta). \tag{45}$$

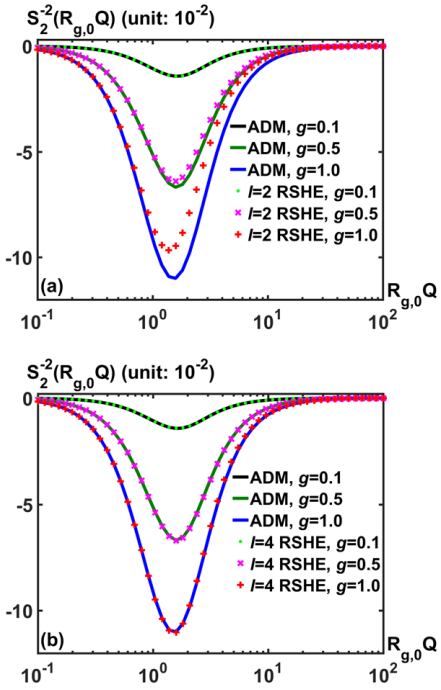

Figure 5. Comparison with between the affine deformation model of polymer and the (a) $l = 2$ and (b) $l = 4$ RSHE of Eq. (37) and Eq. (42).

Because of the high symmetry of the uniaxial extension, the spherical harmonic expansion coefficient S_l^0 of any order l can be in principle obtained from SANS measurement on a single plane parallel to the stretching direction (e.g. the xz plane).

In contrast, as we show here the spherical harmonic expansion coefficients are much more difficult to obtain in the case of shear, even for small ls (2 and 4). Generally speaking, when the microscopic deformation is large, reconstruction of the 3D distorted structures from 2D SAS measurement becomes practically impossible for the shear geometry.

This sharp contrast between shear and extension underscores the fundamental role of the symmetry of flow in the rheo-SANS experiments. On the philosophical level, we generally cannot fully restore the 3D information by examining a finite number of planes. This becomes possible, only when there are further restrictions on the molecular symmetry. For uniaxial extension, the cylindrical symmetry of the deformation significantly simplifies the matter, making the determination of expansion coefficients straightforward. For shear, when the perturbation is sufficiently small, we only need to truncate the expansion at $l = 2$ or $l = 4$. Such a truncation can be equivalently understood as additional symmetry requirement.

The analysis presented in this work has important implications for rheo-SAS experiments. While the shear geometry has been widely used, the pros and cons of different cell designs have not been thoroughly discussed and considered in the context of experimentally accessi-

ble information. For example, we have shown that in the case of truncation at $l = 4$, SAS experiments on the xy-, xz-, and yz-planes yield 5, 2, and 1 LIEs, respectively. While the relative importance of these planes have been intuitively understood previously, this issue has not been addressed rigorously from a mathematical point of view. For the sample rotation method proposed herein, only certain cells are suitable for this approach. On the other hand, although the current discussion has only touched upon simple shear and uniaxial extension, our spherical harmonic expansion approach is certainly applicable to other types of deformation, such as planar and biaxial extensions. Without question the consideration of the deformation symmetry is also critical for the proper design of rheo-SAS experiments in these cases.

To conclude, we discuss the reconstruction of three-dimensional anisotropic structure from small-angle scattering experiments by using spherical harmonic expansion analysis. Because of the low symmetry of the simple shear geometry, the determination of expansion coefficients requires measurements on different planes. When the structural distortion is large, a reconstruction of the 3D $S(\boldsymbol{Q})$ becomes impossible in practice.

To address this challenge, we propose a new approach to rheo-SAS by using a parallel sliding plate shear cell with a central rotary axis along the flow direction. By rotating the shear cell, all the spherical harmonic expansion coefficients can be determined from measurements on two and three special planes, respectively, for $l = 2$ and $l = 4$. For $l = 4$, our proposal is to perform SAS measurement on the xz-plane and subsequently rotate the cell about the x-axis by $\pi/6$ and $\pi/4$, respectively. This design has the potential to bypass the issue of multiple scattering in the traditional Couette flow cell, as it does not require direct measurement on the xy-plane. Lastly, we demonstrate this cell rotation method by using the affine deformation model for polymers. Our approach produces excellent results up to (microscopic) shear strain of 1.0, for RSHE truncated at $l = 4$. We confirm that the higher order terms cannot be neglected, when the mechanical perturbation rises to a certain value.

ACKNOWLEDGMENT

This work was sponsored by the U.S. Department of Energy, Office of Science, Office of Basic Energy Sciences, Materials Sciences and Engineering Division. This research at the Spallation Neutron Source and the Center for Nanophase Materials Sciences of Oak Ridge National Laboratory was sponsored by the Scientific User Facilities Division, Office of Basic Energy Sciences, U.S. Department of Energy. YYW thanks the support by the Laboratory Directed Research and Development Program of Oak Ridge National Laboratory, managed by UT Battelle, LLC, for the U.S. Department of Energy. GRH acknowledges the supports from the National Center for Theoretical Sciences, Ministry of Science and Technology, ROC (Project No. MOST 106-2119-M-007-019) and the Shull Wollan Center during his visit to Oak Ridge National Laboratory.

Appendix A: Rotation about x-axis and z-axis for $l = 4$

In the main text of this paper, we describe a method for $l = 4$ involving cell rotation about the x-axis by two different angles. Alternatively, the extraction of S_l^m for $l = 4$ RSHE can be achieved by rotating plate cell about both the x-axis and z-axis. Similarly, one can find the following nine LIEs:

$$
\begin{aligned}
S_{xz}^{0,0} &= [1,0,0,\sqrt{\frac{5}{3}},0,0,0,\sqrt{\frac{1}{5}},\sqrt{\frac{7}{5}}]\vec{S}^t,\\
S_{xz}^{2,0} &= [0,0,1,-\sqrt{\frac{1}{3}},0,0,0,1,\frac{-2}{\sqrt{7}}]\vec{S}^t,\\
S_{xz}^{4,0} &= [0,0,0,0,0,0,1,\frac{-2}{\sqrt{5}},\frac{1}{\sqrt{35}}]\vec{S}^t,\\
\hat{S}_{xz}^{2,0}(\tfrac{\pi}{4}) &= [0,0,\frac{1}{2},\frac{-\sqrt{3}}{2},0,0,\frac{-3\sqrt{5}}{8},\frac{1}{4},\frac{-19\sqrt{7}}{56}]\vec{S}^t,\\
\hat{S}_{xz}^{2,1}(\tfrac{\pi}{4}) &= [0,\sqrt{2},0,0,\frac{5}{2}\sqrt{\frac{3}{14}},\frac{\sqrt{6}}{4},0,0,0]\vec{S}^t,\\
\hat{S}_{xz}^{4,0}(\tfrac{\pi}{4}) &= [0,0,0,0,0,0,\frac{1}{4},\frac{-3\sqrt{5}}{10},\frac{17\sqrt{35}}{140}]\vec{S}^t,\\
\hat{S}_{xz}^{4,1}(\tfrac{\pi}{4}) &= [0,0,0,0,\frac{-3}{\sqrt{7}},1,0,0,0]\vec{S}^t,\\
\tilde{S}_{xz}^{0,0}(\tfrac{\pi}{4}) &= [1,-\sqrt{\frac{5}{3}},0,0,0,-\sqrt{\frac{1}{5}},0,0,-\sqrt{\frac{7}{5}}]\vec{S}^t,\\
\tilde{S}_{xz}^{2,0}(\tfrac{\pi}{6}) &= [0,\frac{1}{2},1,-\frac{\sqrt{3}}{6},\sqrt{\frac{3}{7}},\frac{-\sqrt{3}}{2},0,\frac{1}{2},\sqrt{\frac{1}{7}}]\vec{S}^t. \quad \text{(A1)}
\end{aligned}
$$

Here, we emphasize that $\tilde{S}_{xz}^{l,m}$ and $\hat{S}_{xz}^{l,m}$ correspond to the rotation along the z- and x-axis, respectively. The set of LIEs are solvable and give the solutions to $\vec{S}$

$$
\begin{aligned}
S_0^0 = &-3.732S_{xz}^{0,0} - 2.955S_{xz}^{2,0} - 5.152S_{xz}^{4,0}\\
&- 5.494\hat{S}_{xz}^{2,0}(\frac{\pi}{4}) + 2.304\hat{S}_{xz}^{2,1}(\frac{\pi}{4}) + 2.179\hat{S}_{xz}^{4,0}(\frac{\pi}{4})\\
&+ 5.643\hat{S}_{xz}^{4,1}(\frac{\pi}{4}) + 4.732\tilde{S}_{xz}^{0,0}(\frac{\pi}{4}) + 5.702\tilde{S}_{xz}^{2,0}(\frac{\pi}{6}),
\end{aligned}
$$

$$
\begin{aligned}
S_2^{-2} = &-1.512S_{xz}^{0,0} - 2.253S_{xz}^{2,0} - 1.260S_{xz}^{4,0}\\
&- 1.803\hat{S}_{xz}^{2,0}(\frac{\pi}{4}) + 0.9717\hat{S}_{xz}^{2,1}(\frac{\pi}{4}) - 1.009\hat{S}_{xz}^{4,0}(\frac{\pi}{4})\\
&+ 2.813\hat{S}_{xz}^{4,1}(\frac{\pi}{4}) + 1.513\tilde{S}_{xz}^{0,0}(\frac{\pi}{4}) + 3.155\tilde{S}_{xz}^{2,0}(\frac{\pi}{6}),
\end{aligned}
$$

$$
\begin{aligned}
S_2^0 = &\ 5.291S_{xz}^{0,0} + 3.553S_{xz}^{2,0} + 7.018S_{xz}^{4,0}\\
&+ 7.643\hat{S}_{xz}^{2,0}(\frac{\pi}{4}) - 2.576\hat{S}_{xz}^{2,1}(\frac{\pi}{4}) - 2.436\hat{S}_{xz}^{4,0}(\frac{\pi}{4})\\
&- 6.309\hat{S}_{xz}^{4,1}(\frac{\pi}{4}) - 5.291\tilde{S}_{xz}^{0,0}(\frac{\pi}{4}) - 6.375\tilde{S}_{xz}^{2,0}(\frac{\pi}{6}),
\end{aligned}
$$

$$
\begin{aligned}
S_2^2 &= 6.545S_{xz}^{0,0} + 3.407S_{xz}^{2,0} + 8.682S_{xz}^{4,0} \\
&+ 8.964\hat{S}_{xz}^{2,0}(\frac{\pi}{4}) - 3.187\hat{S}_{xz}^{2,1}(\frac{\pi}{4}) - 4.673\hat{S}_{xz}^{4,0}(\frac{\pi}{4}) \\
&- 7.806\hat{S}_{xz}^{4,1}(\frac{\pi}{4}) - 6.545\tilde{S}_{xz}^{0,0}(\frac{\pi}{4}) - 7.887\tilde{S}_{xz}^{2,0}(\frac{\pi}{6})
\end{aligned}
$$

$$
\begin{aligned}
S_4^{-4} &= 1.155S_{xz}^{0,0} + 1.721S_{xz}^{2,0} + 0.9621S_{xz}^{4,0} \\
&+ 1.377\hat{S}_{xz}^{2,0}(\frac{\pi}{4}) - 0.2020\hat{S}_{xz}^{2,1}(\frac{\pi}{4}) + 0.7697\hat{S}_{xz}^{4,0}(\frac{\pi}{4}) \\
&- 2.479\hat{S}_{xz}^{4,1}(\frac{\pi}{4}) - 1.155\tilde{S}_{xz}^{0,0}(\frac{\pi}{4}) - 2.409\tilde{S}_{xz}^{2,0}(\frac{\pi}{6}),
\end{aligned}
$$

$$
\begin{aligned}
S_4^{-2} &= 1.309S_{xz}^{0,0} + 1.952S_{xz}^{2,0} + 1.091S_{xz}^{4,0} \\
&+ 1.561\hat{S}_{xz}^{2,0}(\frac{\pi}{4}) - 0.229\hat{S}_{xz}^{2,1}(\frac{\pi}{4}) + 0.8727\hat{S}_{xz}^{4,0}(\frac{\pi}{4}) \\
&- 1.811\hat{S}_{xz}^{4,1}(\frac{\pi}{4}) - 1.309\tilde{S}_{xz}^{0,0}(\frac{\pi}{4}) - 2.732\tilde{S}_{xz}^{2,0}(\frac{\pi}{6}),
\end{aligned}
$$

$$
\begin{aligned}
S_4^{0} &= -2.366S_{xz}^{0,0} - 0.9183S_{xz}^{2,0} - 2.513S_{xz}^{4,0} \\
&- 3.865\hat{S}_{xz}^{2,0}(\frac{\pi}{4}) + 1.152\hat{S}_{xz}^{2,1}(\frac{\pi}{4}) + 1.089\hat{S}_{xz}^{4,0}(\frac{\pi}{4}) \\
&+ 2.822\hat{S}_{xz}^{4,1}(\frac{\pi}{4}) + 2.366\tilde{S}_{xz}^{0,0}(\frac{\pi}{4}) + 2.851\tilde{S}_{xz}^{2,0}(\frac{\pi}{6}),
\end{aligned}
$$

$$
\begin{aligned}
S_4^{2} &= -3.023S_{xz}^{0,0} - 1.173S_{xz}^{2,0} - 4.569S_{xz}^{4,0} \\
&- 4.939\hat{S}_{xz}^{2,0}(\frac{\pi}{4}) + 1.472\hat{S}_{xz}^{2,1}(\frac{\pi}{4}) + 1.711\hat{S}_{xz}^{4,0}(\frac{\pi}{4}) \\
&+ 3.605\hat{S}_{xz}^{4,1}(\frac{\pi}{4}) + 3.023\tilde{S}_{xz}^{0,0}(\frac{\pi}{4}) + 3.643\tilde{S}_{xz}^{2,0}(\frac{\pi}{6}),
\end{aligned}
$$

$$
\begin{aligned}
S_4^{4} &= -2.000S_{xz}^{0,0} - 0.7761S_{xz}^{2,0} - 3.392S_{xz}^{4,0} \\
&- 3.267\hat{S}_{xz}^{2,0}(\frac{\pi}{4}) + 0.9736\hat{S}_{xz}^{2,1}(\frac{\pi}{4}) + 2.611\hat{S}_{xz}^{4,0}(\frac{\pi}{4}) \\
&+ 2.385\hat{S}_{xz}^{4,1}(\frac{\pi}{4}) + 2.000\tilde{S}_{xz}^{0,0}(\frac{\pi}{4}) + 2.409\tilde{S}_{xz}^{2,0}(\frac{\pi}{6}).
\end{aligned}
\tag{A2}
$$

The solutions for S_l^m are much more complicated than the formula presented in the main text, since the z-rotation contains less information than that of x-rotation. Lastly, without tilting many angles about a single axis, it should be feasible to rotate parallel-plate cell about different axes to gain additional information for extracting high order terms, for example, the $l = 6$ terms.

[1] D. J. Evans, H. J. M. Hanley, and S. Hess, Phys. Today **37**, 26 (1984).
[2] M. Kröger, Physics reports **390**, 453 (2004).
[3] X. Cheng, J. H. McCoy, J. N. Israelachvili, and I. Cohen, Science **333**, 1276 (2011).
[4] J. Zausch and J. Horbach, EPL, **88**, 60001 (2009).
[5] N. Koumakis, M. Laurati, S. U. Egelhaaf, J. F. Brady, and G. Petekidis, Phys. Rev. Lett. **108**, 098303 (2012).
[6] K.J. Mutch, M. Laurati, C.P. Amann, M. Fuchs, S.U. Egelhaaf, Eur. Phys. J. Special Topics **222**(11), 2803 (2013).
[7] N. Koumakis, M. Laurati, A.R. Jacob, K.J. Mutch, A. Abdellali, A.B. Schofield, S.U. Egelhaaf, J.F. Brady, and G. Petekidis, J. Rheol. **60**, 603623 (2016).
[8] D. J. Evans and H. J. M. Hanley, Phys. Rev. A **20**, 1648 (1979).
[9] H. J. M. Hanley and D. J. Evans, J. Chem. Phys. **76**, 3225 (1982).
[10] S. Hess and H. J. M. Hanley, Phys. Rev. A **25**, 1801 (1982).
[11] H. J. M. Hanley, J. C. Rainwater, and S. Hess, Phys. Rev. A **36**, 1795 (1987).
[12] J. F. Morris and B. Katyal, Physics of Fluids **14**, 1920 (2002).
[13] N. A. Clark and B. J. Ackerson, Phys. Rev. Lett. **44**, 1005 (1980).
[14] B. J. Ackerson and N. A. Clark, Physica A **118**, 221 (1983).
[15] Y. Suzuki, J. Haimovich, and T. Egami, Phys. Rev. B **35**, 2162 (1987).
[16] N. J. Wagner and W. B. Russel, Physics of Fluids A: Fluid Dynamics **2**, 491 (1990).
[17] N. J. Wagner and B. J. Ackerson, J. Chem. Phys. **97**, 1473 (1992).
[18] B. J. Maranzano and N. J. Wagner, J. Chem. Phys. **117**, 10291 (2002).
[19] A. K. Gurnon and N. J. Wagner, J. Fluid. Mech. **769**, 242 (2015).
[20] Z. Wang, T. Iwashita, L. Porcar, Y. Wang, Y. Liu, L. E. Sanchez-Diaz, B. Wu, T. Egami, and W.-R. Chen, arXiv preprint arXiv:1611.03135 (2016).
[21] Z. Wang, C. N. Lam, W.-R. Chen, W. Wang, J. Liu, Y. Liu, L. Porcar, C. B. Stanley, Z. Zhao, K. Hong, and Y. Wang, Phys. Rev. X, in press (2017).
[22] Joseph Ivanic and Klaus Ruedenberg, J. Phys. Chem., **100**: 6342-6347 (1996).
[23] Miguel A. Blanco, M. Flrez, M. Bermejo, J. Mol. Struc-THEOCHEM, **419**: 19-27 (1997).
[24] D.A. Varshalovich, A.N. Moskalev, V.K. Khersonskii, Quantum Theory of Angular Momentum, 1st edn, World Scientific, Singapore, 1988.